Wireless Power Transfer

ARTICLE

Open Access

https://doi.org/10.48130/wpt-0024-0004

Wireless Power Transfer **2024**, 11: e004

Calculation method of mutual inductance of circular coils with bilateral convex toroidal magnetic medium in WPT system with horizontal misalignment

Changxuan Hu[1], Zhongqi Li[1,2,3*], Lingjun Kong[2], Jianbin Wang[1] and Chenxi Zhang[1]

[1] *College of Railway Transportation, Hunan University of Technology, Zhuzhou 412007, China*
[2] *College of Electrical and Information Engineering, Hunan University of Technology, Zhuzhou 412007, China*
[3] *College of Electrical and Information Engineering, Hunan University, Changsha 410082, China*
* Corresponding author, E-mail: my3eee@126.com

Abstract

Accurately calculating mutual inductance is crucial for achieving efficient and reliable wireless power transfer systems. However, when horizontal displacement occurs in double-sided magnetic coils, the mutual inductance values are typically obtained using finite element software, lacking a simple analytical formula for calculation. Additionally, magnetic materials are costly, and there's still room for optimizing disc-type magnetic structures. Therefore, this paper proposes a magnetic vector potential position equivalent method and derives an analytical solution for mutual inductance of circular coils with bilateral convex toroidal bounded magnetic media. The magnetic vector potential in each region can be derived, based on Maxwell's equations and combined with boundary conditions. Utilizing the position equivalent method enables rapid calculation of mutual inductance for coaxial and horizontally displaced scenarios on the receiving end. Comparison between calculated mutual inductance values and finite element simulation, along with experimental measurements, demonstrates an error within 4.23% and a calculation speed 70 times faster than simulation. Experimental validation shows that the mutual inductance of the convex toroidal magnetic structure can reach more than 97.75% of the mutual inductance of the disc-type magnetic structure while saving 15% of magnetic material.

Citation: Hu C, Li Z, Kong L, Wang J, Zhang C. 2024. Calculation method of mutual inductance of circular coils with bilateral convex toroidal magnetic medium in WPT system with horizontal misalignment. *Wireless Power Transfer* 11: e004 https://doi.org/10.48130/wpt-0024-0004

Introduction

The rapid development of electrification is driving wireless power transfer (WPT) technology as a research field with great potential. This type of electrical energy transmission method does not require physical contact and thus is characterized by flexibility and safety. Compared with the traditional wired method, wireless power transfer is gradually demonstrating its advantages in the fields of electric power systems, transportation, aerospace, underwater exploration, home office, and medical devices[1–10]. Efficiency and cost are key considerations when designing and optimizing magnetically coupled wireless energy transmission systems. In practice, the receiving coil will inevitably sustain horizontal misalignment, which will affect the mutual inductance between the coils, thus affecting the transmission efficiency, and the calculation of mutual inductance between the coils is the basis for exploring the change rule of mutual inductance with horizontal misalignment. Therefore, it is of significance to study the mutual inductance calculation method between the transmitting and receiving coil.

Currently, researchers usually use finite element method (FEM) simulation software to obtain the mutual inductance value, but this method has the disadvantages of large computation and is time-consuming. Especially in the case of complex coil distribution or a large number of turns, the simulation may take several hours. On the other hand, considerable progress has been made in the analytical calculation of coil mutual inductance. The utilization of elliptic integrals for calculating the mutual inductance of circular coils in air, whether coaxial or non-coaxial, was proposed by researchers, offering a combination of swiftness and precision[11,12]. Conway expressed the mutual inductance of non-coaxial circular coils in air in the form of Bessel integrals[13]. Hurley et al. extended the mutual inductance formula for single-turn coils to derive an expression for the mutual inductance of coaxial coils in air, which is easily solved by numerical integration[14]. Liu et al. derived the mutual inductance formula for a circular coil at any position based on the Euler angle based on the Neumann integral[15]. However, none of the above-studied models considered the case of magnetic media.

The addition of magnetic media at the coil edges has a significant effect on enhancing the mutual inductance between the coils. For the calculation of mutual inductance with magnetic media, Hurley & Duffy derived analytical expressions for the coaxial mutual inductance of a circular coil with infinite thickness and finite thickness of magnetic media with the help of magnetic vector potential[16], however, the magnetic media is unbounded in the plane. Luo & Wei derived analytical expressions for the mutual inductance of a circular coil coaxial and horizontal misalignment with an unbounded magnetic medium based on the Fourier-Bessel transform[17]. Zhang et al. obtained analytical formulas for the mutual inductance between circular coils at any position of an unbounded double-layer magnetic medium based on the coordinate transformation method[18]. All the above derivations are based on the premise that the magnetic medium material has an infinite plane and a good approximation can only be obtained if the radius of the magnetic medium is twice as large as the coil, which has many obstacles in practical applications.

To solve the mutual inductance calculation problem of circular coils with bounded magnetic media, the researchers utilized the regional eigenfunctions and introduced the truncation domain to express the mutual inductance of circular coils with bounded magnetic media in the form of level summation[19,20]. But the

magnetic media is only for unilateral cases, which is incompatible with practical application. Chen et al. established an analytical mapping from geometrical parameters to inductance parameters for finite large magnetic conductors based on the principles of magnetic circuit magnetic reluctance[21] but only in the case when the coil is coaxial is considered, the analytical solution of mutual inductance at the misalignment of the receiving side is not given, and no consideration has been given to material savings. The performance of the cut-hole type and the flat plate type structure, and the ring type and the disc-type structure were compared in terms of coupling and the results proved to be useful for saving magnetic materials[22,23]. In summary, the problem of mutual inductance calculation, when the horizontal misalignment occurs on the receiving side of a bounded magnetic medium with bilateral sides, has not been solved yet, and it is achievable that bilateral magnetic dielectric materials can be reduced in consumption.

This paper presents a circular coil model with bilateral bounded convex magnetic material rings, as illustrated in Fig. 1. By employing the method of magnetic vector potential position equivalence, the issue of mutual inductance calculation is addressed when the receiver side is coaxial and when there is horizontal misalignment. Firstly, this method divides the model into regions and, based on Maxwell's equations and boundary conditions compute the magnetic vector potentials in each region, deriving analytical expressions for mutual inductance when the receiver side is coaxial. Secondly, utilizing the method of position equivalence, the magnetic material after horizontal displacement is equivalent to the average effect of two coaxial magnetic materials with different radii, so that analytical expressions for mutual inductance are derived for horizontal misalignment. Finally, the calculated values of mutual inductance are compared with finite element simulation values and experimental values.

Mutual inductance calculation at coaxial

To achieve a similar effect to the enhanced mutual inductance of disc-type magnetic media and to save the use of magnetic media consumables, a single-turn circular coil model with a double-sided bounded convex toroidal magnetic media is constructed by adding a raised portion of the inner edge to the inner ring of the toroidal magnetic media material and a cross-section of the model is shown in Fig. 2.

A cylindrical coordinate system (r, φ, z) is established with the center of the upper surface of the magnetic medium on the emission side as the origin. The symbol μ_r represents the relative magnetic permeability of the magnetic materials, and σ denotes the conductivity, both of which are linear, homogeneous, and isotropic.

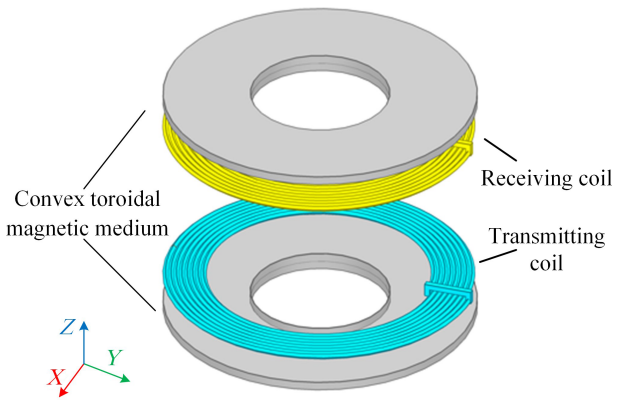

Fig. 1 Simulated model of bilateral convex toroidal magnetic media.

Taking the magnetic medium on the transmitting side as an example, r_1, and r_3 are the inner and outer diameters of the annular part, and its thickness is c_1, and the outer diameter of the raised part along the inner edge is r_2, and its thickness is c_2. The radius of the transmitting coil is r_p, and the height at which it is situated is z_p. The radius of the receiving coil is r_s, and the height at which it is situated is z_s. The rest of the medium is air, the permeability of which is set to be the vacuum permeability μ_0, and h is the truncated region radius in the model. region radius. Along the z-axis increasing direction, the model is divided into eight regions according to the planes $z = z_1$, $z = z_2$, $z = 0$, $z = z_p$, $z = z_3$, $z = z_4$, $z = z_5$ as shown in Fig. 2.

Magnetic vector position generalizations by region

In electromagnetism, Maxwell's equations relating the magnetic induction $\boldsymbol{B}$ and the magnetic field strength $\boldsymbol{H}$ are:

$$\begin{cases} \nabla \times \boldsymbol{H} = \boldsymbol{J} + \dfrac{\partial \boldsymbol{D}}{\partial t} \\ \nabla \cdot \boldsymbol{B} = 0 \end{cases} \tag{1}$$

where, $\boldsymbol{J}$ is the conduction current density and $\boldsymbol{D}$ is the electric displacement vector. Conventional WPT systems usually operate at an operating frequency of 79–90 kHz, a frequency range in which the system can be considered as an ideal magnetically quasi-static system, and therefore the displacement current can be neglected. Introducing the magnetic vector potential $\boldsymbol{A}$, from the Coulomb norm, Eqn (1) is reduced to the Poisson equation:

$$\nabla^2 \boldsymbol{A} = -\mu \boldsymbol{J} \tag{2}$$

where, μ is the magnetic permeability of the material. The excitation current flowing through the transmitting coil in the model has an amplitude of I and an angular frequency of ω. The direction of the current is along the φ direction, inducing a magnetic vector potential $\boldsymbol{A}$ in the same direction, i.e., $\boldsymbol{A} = \boldsymbol{A}_\varphi$, and from Eqn (2), $\boldsymbol{A}$ satisfies:

$$\frac{\partial^2 A}{\partial^2 r} + \frac{1}{r}\frac{\partial A}{\partial r} + \frac{\partial^2 A}{\partial^2 z} - \frac{A}{r^2} - j\omega\mu\sigma A = -\mu I \delta\left(r - r_p\right)\delta\left(z - z_p\right) \tag{3}$$

where, δ is the impulse excitation function. The magnetic vector potential expression is solved in the column coordinate system in separated variables as:

$$A(r,z) = \sum_{i=1}^{\infty} \left[A_{mn} J_1(\alpha_i r) + B_{mn} Y_1(\alpha_i r)\right]\left(C_m e^{\beta_i z} + D_m e^{-\beta_i z}\right) \tag{4}$$

in the above expression, the subscript i is from 1 to ∞, α_i, β_i are the eigenvalues, and $\alpha_i = (\beta_i^2 + j\omega\mu\sigma)^{1/2}$, $J_1(\alpha_i r)$, $Y_1(\alpha_i r)$ represent the first-order Bessel function and the first-order Neumann function, respectively. A_{mn}, B_{mn}, C_m, and D_m are the regionally unknown coefficients associated with the eigenvalues. They can be obtained from the

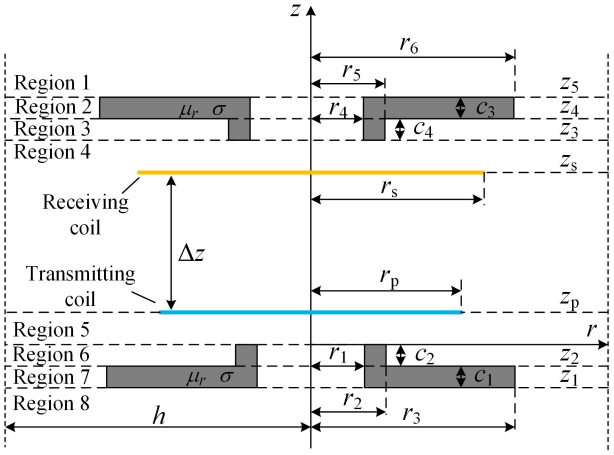

Fig. 2 Cross-sectional view of the model.

continuity of the magnetic induction $\boldsymbol{B}$ in the normal direction in the neighboring medium and the continuity of the magnetic field strength $\boldsymbol{H}$ in the tangential direction. The subscript m denotes the location of the region and n denotes the location of the sublayer in the region.

The expression for the magnetic vector potential in each region is determined by the distribution of sublayers inside the region. Regions 1, 4, 5, and 8 all have air sublayers inside, and the Neumann function diverges at $Y_1(\alpha_i r)$ at $r = 0$. However, the magnetic vector potential is finite here, so the $Y_1(\alpha_i r)$ term is discarded, and therefore the magnetic vector potentials for regions 1, 4, 5, and 8 are derived as:

$$A_1(r,z) = \sum_{i=1}^{\infty} J_1(k_i r) D_1 \mathrm{e}^{-k_i z} \tag{5}$$

$$A_4(r,z) = \sum_{i=1}^{\infty} J_1(k_i r)\left(C_4 \mathrm{e}^{k_i z} + D_4 \mathrm{e}^{-k_i z}\right) \tag{6}$$

$$A_5(r,z) = \sum_{i=1}^{\infty} J_1(k_i r)\left(C_5 \mathrm{e}^{k_i z} + D_5 \mathrm{e}^{-k_i z}\right) \tag{7}$$

$$A_8(r,z) = \sum_{i=1}^{\infty} J_1(k_i r) C_8 \mathrm{e}^{k_i z} \tag{8}$$

where, k_i is the eigenvalue of the aforementioned region. By utilizing the disappearance of the magnetic vector potential at the truncation radius $r = h$, i.e., $J_1(k_i h) = 0$, the eigenvalue k_i can be determined.

Regions 2, 3, 6, and 7 contain two types of media: air media and magnetic media. Take Region 2 as an example:

(1) In the range of $0 \le r < r_4$ is the air sublayer, and its magnetic vector potential $\boldsymbol{A}_2^{air1}$ is represented as:

$$A_2^{air1}(r,z) = \sum_{i=1}^{\infty} J_1(p_{1i} r)\left(C_2 \mathrm{e}^{p_{1i} z} + D_2 \mathrm{e}^{-p_{1i} z}\right) \tag{9}$$

(2) In the range of $r_4 \le r < r_6$ is the magnetic medium sublayer, and its magnetic vector potential $\boldsymbol{A}_2^{fer2}$ is represented as:

$$A_2^{fer2}(r,z) = \sum_{i=1}^{\infty} \left[A_{22} J_1(q_{1i} r) + B_{22} Y_1(q_{1i} r)\right]\left(C_2 \mathrm{e}^{p_{1i} z} + D_2 \mathrm{e}^{-p_{1i} z}\right) \tag{10}$$

(3) In the range of $r_6 \le r < h$ is also the air sublayer, and its magnetic vector potential $\boldsymbol{A}_2^{air3}$ is expressed as:

$$A_2^{air3}(r,z) = \sum_{i=1}^{\infty} \left[A_{23} J_1(p_{1i} r) + B_{23} Y_1(p_{1i} r)\right]\left(C_2 \mathrm{e}^{p_{1i} z} + D_2 \mathrm{e}^{-p_{1i} z}\right) \tag{11}$$

where, p_{1i}, q_{1i} are the eigenvalues of Region 2 and satisfy the relation $q_{1i} = (p_{1i}^2 + \mathrm{j}\omega\mu\sigma)^{1/2}$, $\boldsymbol{A}_2^{air3}$ converges to 0 at $r = h$, and the eigenvalue p_{1i} can be found by Eqn (12).

$$A_{23} J_1(p_{1i} h) + B_{23} Y_1(p_{1i} h) = 0 \tag{12}$$

The magnetic vector potential generalization for this region consists of a combination of $\boldsymbol{A}_2^{air1}$, $\boldsymbol{A}_2^{fer2}$, and $\boldsymbol{A}_2^{air3}$. Similarly, the magnetic vector potential expressions for regions 3, 6, and 7 are combinations of the magnetic vector potentials of the sublayers within each region and can be derived similarly.

Boundary conditions

In the cylindrical coordinate system, the relationship between the magnetic induction $\boldsymbol{B}$, the magnetic field strength $\boldsymbol{H}$, and the magnetic vector potential $\boldsymbol{A}$ can be described as:

$$\begin{cases} B_z = \mu H_z = \dfrac{1}{r}\dfrac{\partial (r \cdot A)}{\partial r} \\ B_r = \mu H_r = -\dfrac{\partial A}{\partial z} \end{cases} \tag{13}$$

Therefore, it is necessary to consider the relationship between the magnetic vector potentials at the two positions, as shown in Fig. 3, where the derivatives of the magnetic vector potentials at the dielectric demarcation surface must satisfy the continuity condition along the demarcation interface to ensure the continuity of the electromagnetic field.

In the Fig. 3, $\boldsymbol{A}_a$ and $\boldsymbol{A}_b$ are the magnetic vector potentials in medium a and medium b. μ_a and μ_b are the magnetic permeability of medium a and medium b.

At the boundary interface between the air layer and the magnetic medium layer in Region 2, located at $r = r_1$, the continuity of field quantities yields:

$$J_1(q_{1i} r_1) = \left[A_{22} J_1(q_{1i} r_1) + B_{22} Y_1(q_{1i} r_1)\right] \tag{14}$$

$$\mu_r p_{1i} J_0(p_{1i} r_1) = q_{1i}\left[A_{22} J_0(q_{1i} r_1) + B_{22} Y_0(q_{1i} r_1)\right] \tag{15}$$

The association can be solved for the area coefficients A_{22} and B_{22} as:

$$A_{22} = \frac{\mu_r p_{1i} J_0(p_{1i} r_1) Y_1(q_{1i} r_1) - q_{1i} J_1(p_{1i} r_1) Y_0(q_{1i} r_1)}{q_{1i} J_0(q_{1i} r_1) Y_1(q_{1i} r_1) - q_{1i} J_1(q_{1i} r_1) Y_0(q_{1i} r_1)} \tag{16}$$

$$B_{22} = \frac{q_{1i} J_0(q_{1i} r_1) J_1(p_{1i} r_1) - \mu_r p_{1i} J_0(p_{1i} r_1) J_1(q_{1i} r_1)}{q_{1i} J_0(q_{1i} r_1) Y_1(q_{1i} r_1) - q_{1i} J_1(q_{1i} r_1) Y_0(q_{1i} r_1)} \tag{17}$$

The coefficients A_{23} and B_{23} can be found in the same way, and the corresponding coefficients for Regions 3, 6, and 7 are obtained in the same way.

Coaxial mutual inductance expressions

To calculate the magnetic flux of the receiving coil, an expression for the magnetic vector potential of the region where the receiving coil is located is required. Associating the magnetic vector potentials from Region 1 to Region 8 and utilizing the boundary conditions at the interfaces $z = z_1$, $z = z_2$, $z = 0$, $z = z_p$, $z = z_3$, $z = z_4$, $z = z_5$, there are:

$$\frac{\partial A_i(r,z)}{\partial z} = \frac{\partial A_{i+1}(r,z)}{\partial z} \tag{18}$$

$$\frac{\partial A_i(r,z)}{\partial z}\Big|_{z=z_n} - \frac{\partial A_{i+1}(r,z)}{\partial z}\Big|_{z=z_n} = -u_0 J \tag{19}$$

The magnetic vector $\boldsymbol{A}$ contains the Bessel function and with the help of the orthogonality of the Bessel function, multiplying the Region 1 magnetic vector $\boldsymbol{A}_1$ by $J_1(k_i r)\cdot r$ and integrating from 0 to h yields:

$$\int_0^h \sum_{i=1}^{\infty} D_1 \mathrm{e}^{-k_i z} J_1(k_i r) J_1(k_i r)\, r \mathrm{d}r = \sum_{i=1}^{\infty} \frac{h^2}{2} D_1 \mathrm{e}^{-k_i z} J_2(k_i h) \tag{20}$$

Doing the same for both sides of Eqns (18) & (19) and noting the eigenvalues of Regions 3, 6, and 7 as p_{2i}, p_{3i}, and p_{4i}, the equation

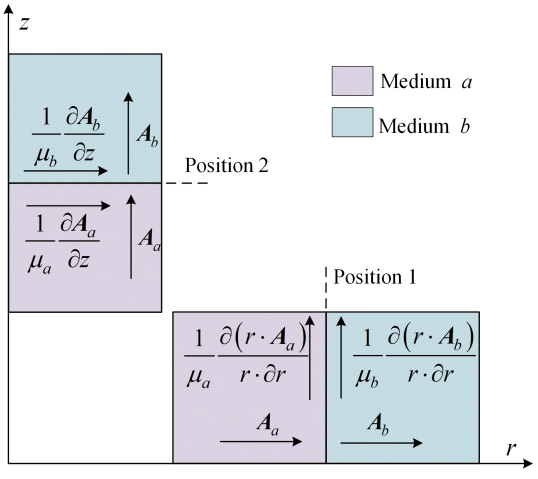

Fig. 3 Magnetic vector potential at interface in two positions.

reduces to:

$$e^{-k_i z_5} D_1 E_{10} = (e^{p_{1i} z_5} C_2 + e^{-p_{1i} z_5} D_2) E_{20} \tag{21}$$

$$-k_i e^{-k_i z_5} D_1 E_{10} = p_{1i} (e^{p_{1i} z_5} C_2 - e^{-p_{1i} z_5} D_2) E_{21} \tag{22}$$

$$(e^{p_{1i} z_4} C_2 + e^{-p_{1i} z_4} D_2) E_{20} = (e^{p_{1i} z_4} C_3 + e^{-p_{1i} z_4} D_3) E_{30} \tag{23}$$

$$p_{1i} (e^{p_{1i} z_4} C_2 - e^{-p_{1i} z_4} D_2) E_{21} = p_{2i} (e^{p_{2i} z_4} C_3 - e^{-p_{2i} z_4} D_3) E_{31} \tag{24}$$

$$(e^{p_{2i} z_3} C_3 + e^{-p_{2i} z_3} D_3) E_{30} = \left(e^{k_i z_3} C_4 + e^{-k_i z_3} D_4\right) E_{40} \tag{25}$$

$$p_{2i} (e^{p_{2i} z_3} C_3 - e^{-p_{2i} z_3} D_3) E_{31} = k_i \left(e^{k_i z_3} C_4 - e^{-k_i z_3} D_4\right) E_{40} \tag{26}$$

$$\left(e^{k_i z_p} C_4 + e^{-k_i z_p} D_4\right) E_{40} = \left(e^{k_i z_p} C_5 + e^{-k_i z_p} D_5\right) E_{50} \tag{27}$$

$$k_i \left(e^{k_i z_p} C_5 - e^{-k_i z_p} D_5\right) E_{50} - k_i \left(e^{k_i z_p} C_4 - e^{-k_i z_p} D_4\right) E_{40} = \mu_r r_p I J_1 \left(k_i r_p\right) \tag{28}$$

$$(C_5 + D_5) E_{50} = (C_6 + D_6) E_{60} \tag{29}$$

$$k_i (C_5 - D_5) E_{50} = p_{3i} (C_6 - D_6) E_{61} \tag{30}$$

$$(e^{p_{3i} z_2} C_6 + e^{-p_{3i} z_2} D_6) E_{60} = (e^{p_{4i} z_p} C_7 + e^{-p_{4i} z_p} D_7) E_{70} \tag{31}$$

$$p_{3i} (e^{p_{3i} z_2} C_6 - e^{-p_{3i} z_2} D_6) E_{61} = p_{4i} (e^{p_{4i} z_p} C_7 - e^{-p_{4i} z_p} D_7) E_{71} \tag{32}$$

$$(e^{p_{4i} z_1} C_7 + e^{-p_{4i} z_1} D_7) E_{70} = e^{k_i z_1} E_{80} \tag{33}$$

$$p_{4i} (e^{p_{4i} z_1} C_7 - e^{-p_{4i} z_1} D_7) E_{71} = e^{k_i z_1} E_{80} \tag{34}$$

In the equation, E_{10}–E_{80} denotes the intermediate variable in the integral form and E_{10}, E_{40}, E_{50}, E_{80} are equal and the E_{10} expression is:

$$E_{10} = \int_0^h J_1 (k_i r) J_1 (k_i r) r dr \tag{35}$$

E_{20}, E_{21} are expressed as:

$$E_{20} = \int_0^{r_4} J_1 (p_{1i} r) J_1 (k_i r) r dr + \int_{r_4}^{r_6} [A_{22} J_1 (q_{1i} r) + B_{22} Y_1 (q_{1i} r)] J_1 (k_i r) r dr + \int_{r_6}^{h} [A_{23} J_1 (p_{1i} r) + B_{23} Y_1 (p_{1i} r)] J_1 (k_i r) r dr \tag{36}$$

$$E_{21} = \int_0^{r_4} J_1 (p_{1i} r) J_1 (k_i r) r dr + \frac{1}{\mu_r} \int_{r_4}^{r_6} [A_{22} J_1 (q_{1i} r) + B_{22} Y_1 (q_{1i} r)] J_1 (k_{1i} r) r dr + \int_{r_6}^{h} [A_{23} J_1 (p_{1i} r) + B_{23} Y_1 (p_{1i} r)] J_1 (k_i r) r dr \tag{37}$$

E_{30}, E_{31}, E_{60}, E_{61}, E_{70}, and E_{71} can be listed based on the distribution of neutron layers in neighboring regions and the regularity of boundary conditions.

In the actual solution, choosing an appropriate upper limit of the eigenvalue is crucial to maintaining the computational accuracy and simplifying the process. In this paper, the upper limit value n is selected to be 35, and the unknown coefficients D_1–D_7 and C_2–C_8 can be solved by utilizing Clem's law in matrix operations after converting Eqns (21)–(34) into matrix form.

The receiving coil is located in Region 4, so the magnetic flux Φ of the receiving coil can be obtained by calculating the integral of the magnetic vector potential along the receiving coil in Region 4, as Eqn (38):

$$\Phi = \oint A_4 (r_s, z_s) dl \tag{38}$$

The mutual inductance M between a single-turn transmitting coil and a single-turn receiving coil is denoted by:

$$M = \frac{\Phi}{I} = \frac{2\pi r_s}{I} A_4 (r_s, z_s) \tag{39}$$

The transmitting and receiving coils are multi-turn wound helical coils, which can be approximated as a superposition of multi-turn circular coils. Therefore, the total mutual inductance M_{total} can be expressed as:

$$M_{total} = \sum_{m=1}^{N_p} \sum_{g=1}^{N_s} M_{mg} \tag{40}$$

N_p and N_s respectively represent the total number of turns of the transmitting coil and the receiving coil. M_{mg} represents the mutual inductance between the m-th turn of the transmitting coil and the g-th turn of the receiving coil. Equation (40) can be used as a formula for calculating the mutual inductance between the coils when the receiving side is placed coaxially with the transmitting side.

Positional equivalence method for solving horizontal misalignment mutual inductance expressions

In practice, there will inevitably be a horizontal misalignment on the receiving side of a wireless energy transmission system. Due to the presence of a magnetic medium on the receiving side, the horizontal misalignment will destroy the cylindrical symmetry of the model, making it impossible to continue to calculate the mutual inductance value using the original method. Therefore, this section proposes a positional equivalence method for deriving the mutual inductance calculation formula for horizontal misalignment. Figure 4 illustrates the four steps of calculating the mutual inductance for horizontal misalignment using the positional equivalence method.

For the model proposed in this paper, when the horizontal misalignment distance is d_1, the model misalignment diagram is shown in Fig. 5.

The principle of the position equivalence method is to equivalently represent the effect of the magnetic medium on the receiving side after horizontal displacement as the average effect of two magnetic media positioned coaxially with different radii. This magnetic medium structure serves as a substitute for disc-type magnetic medium structures, so only the equivalence of the magnetic medium's outer radius needs to be considered. The equivalent

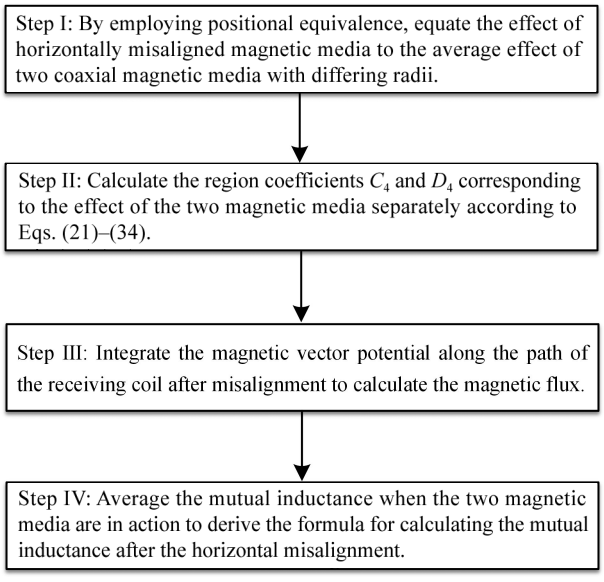

Fig. 4 Step-by-step calculation of mutual inductance with horizontal misalignment.

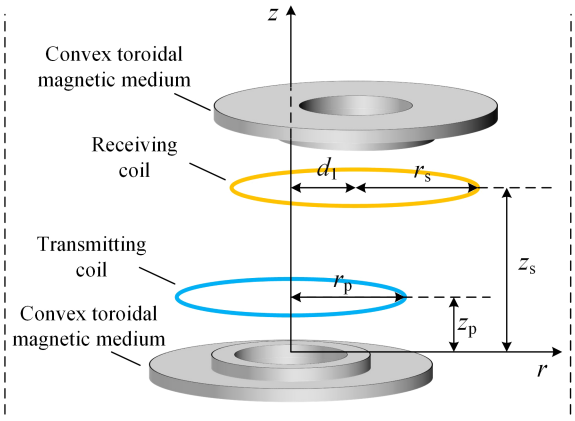

Fig. 5 Horizontal misalignment model diagram.

process of a magnetic medium with an outer radius of r_6 is illustrated in Fig. 6. r_{eq1} represents the radius of the magnetic medium after equivalence, which is smaller, and r_{eq2} represents the radius of the magnetic medium after equivalence, which is larger. The magnetic material remains the same before and after equivalence.

The above equivalent process coordinate relationship can be described by Eqn (41):

$$\begin{bmatrix} r_{eq1} \\ r_{eq2} \end{bmatrix} = \begin{bmatrix} 1 & -d_1 \\ 1 & d_1 \end{bmatrix} \begin{bmatrix} r_6 \\ 1 \end{bmatrix} \tag{41}$$

Replace r_6 with the equivalent magnetic medium radii r_{eq1} and r_{eq2} in turn, and reintroduce them into the above system of Eqns (21)–(34) according to the steps, which can be solved for the new area coefficients C_4 and D_4, respectively.

Figure 7 illustrates a top view of the transmitting coil and the receiving coil at a horizontal misalignment distance of d_1. In the figure, *dl* represents a certain integral line element of the receiving coil, which is oriented at an angle to the magnetic vector potential of α. The angle between the radial direction over the line element and the opposite direction of the *r*-axis is noted as θ. d_2 is the distance between the location of the transmitter coil's center of circle and the line element, which is given by the cosine equation

$$d_2 = \sqrt{{d_1}^2 + {r_s}^2 - 2d_1 r_s \cos\theta} \tag{42}$$

The magnetic flux of the receiving coil is the integral of $\boldsymbol{A}_4(r, z_s)$ along the receiving coil and the flux Φ is expressed as:

$$\Phi = \oint A_4(r, z_s)\cos\alpha dl \tag{43}$$

The mutual inductance *M* between the multi-turn transmitting coil and the multi-turn receiving coil at horizontal misalignment is:

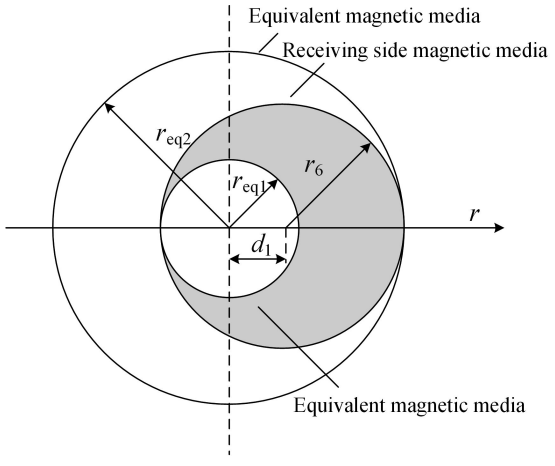

Fig. 6 Equivalent diagram of magnetic media positions.

$$M = \frac{1}{I}\sum_{m=1}^{N_p}\sum_{s=1}^{N_s}\sum_{i=1}^{n}\int_0^{2\pi} J_1(k_i r)\left(C_4 e^{k_i z_s} + D_4 e^{-k_i z_s}\right) r_s \frac{r_s - d_1\cos\theta}{d_2} d\theta \tag{44}$$

The mutual inductance M_{total} calculated after using the positional equivalence method is:

$$M_{total} = \frac{M_{eq1} + M_{eq2}}{2} \tag{45}$$

where M_{eq1} and M_{eq2} represent the mutual inductance when two coaxial magnetic media with different radius sizes act separately after equivalence, which can be derived from Eqn (44). Equation (45) describes the expression for calculating the mutual inductance after the horizontal misalignment of the receiving side.

Verification

To verify the accuracy of the calculation method, the mutual inductance calculation program is written using Matlab software, and the mutual inductance calculation values are obtained. Simultaneously, the model is drawn using Ansys Maxwell finite element software and the mutual inductance simulation values are obtained. By building an experimental platform, the experimental value of the mutual inductance is obtained by using an impedance analyzer. The calculated values of mutual inductance are compared with the simulated and experimental values to analyze the errors in the three cases of different transmission distances on the receiving side, different distances with horizontal misalignment, and changes in the number of turns of the receiving coil. On this basis, this paper further compares the mutual inductance values in the case of convex toroidal media structure and disc-type media structure, the time consumed for calculating mutual inductance and simulating mutual inductance, and the differences of mutual inductance calculation methods in the domestic and foreign research literature.

The experimental test setup built in this paper is shown in Fig. 8, and the detailed parameters of the coil and magnetic media are shown in Table 1.

Figure 9a–c shows the experimental procedure at different transmission distances on the receiving side, at different distances of horizontal misalignment, and changes in the number of turns of the receiving coil.

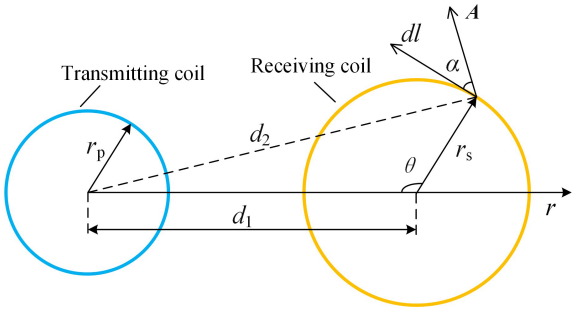

Fig. 7 Top view of coil with horizontal misalignment.

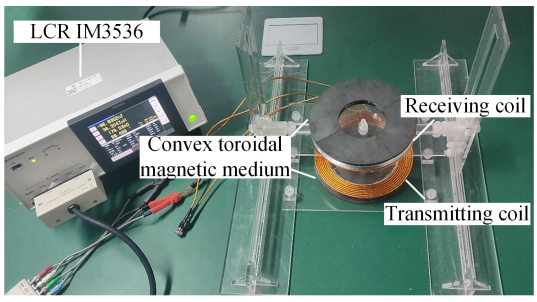

Fig. 8 Experimental test setup.

Table 1. Coil and magnetic media parameters.

Parameters	Value
Coil radius change	0.1 mm
Copper wire diameter	3 mm
Height of receiving coil, z_s	22–112 mm
Coil to medium distance, z_p	12 mm
Turns of transmitting coil, N_p	8
Turns of receiving coil, N_s	9
Transmitting coil inner radius, r_p	62 mm
Receiving coil inner radius, r_s	65.1 mm
Conductivity of mag. media, σ	0.01 S/m
Relative permeability of mag. media, μ_r	2,800
Thickness of toroidal mag. media, c_1 (c_3)	5 mm
Thickness of convex mag .media, c_2 (c_4)	5 mm
Inner diameters of toroidal mag. media, r_1 (r_4)	35 mm
Outer radius of toroidal mag. media, r_3 (r_6)	90 mm
Outer radius of convex mag. media, r_2 (r_5)	35.15 mm

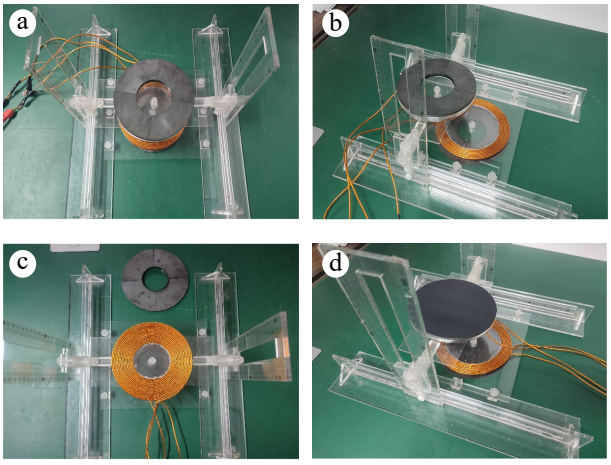

Fig. 9 Diagram of different experimental processes. (a) Transmission distance variation; (b) horizontal misalignment; (c) variation of turns; (d) disc-type comparison.

The experiment uses an impedance analyzer IM3536 for measuring the mutual inductance values. The current frequency is set to 85 kHz and the measurement principle is illustrated in Fig. 10. The specific measurement procedure is as follows: when the terminals of the receiving coil are connected forwardly with the terminals of the transmitting coil, the forward series mutual inductance L_1 can be obtained as $L_1 = (L_p + L_s + 2M)$; when connected in reverse, the reverse series mutual inductance L_2 can be obtained as $L_2 = (L_p + L_s - 2M)$. Wherein, L_p and L_s represent the self-inductance values of the transmitting and receiving coils respectively, and the mutual inductance value M can be calculated using the formula $M = (L_1 - L_2)/4$.

For analysis, the simulation error coefficient ε_1 and the experimental error coefficient ε_2 are defined as:

$$\varepsilon_1 = \frac{|M_s - M_c|}{M_c} \times 100\% \tag{46}$$

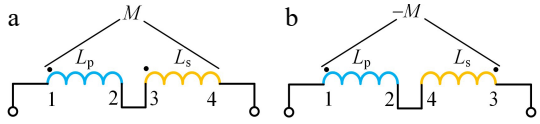

Fig. 10 Mutual inductance measurement schematic. (a) Series connection; (b) inverted series connection.

$$\varepsilon_2 = \frac{|M_e - M_c|}{M_c} \times 100\% \tag{47}$$

where, M_s is the simulated value of mutual inductance, M_e is the experimental value of mutual inductance and M_c is the calculated value of mutual inductance.

Different transmission distances

In the experiments with different transmission distances, the receiving side was set to be placed coaxially with the transmitting side and the receiving coil and magnetic medium were moved along the z-axis positive direction in steps of 10 mm. The initial height of the receiving coil is set to z_s = 22 mm, and the calculated, simulated, and experimental values of mutual inductance for Δz from 10 to 100 mm are recorded step by step. Figure 11 shows the schematic of the model at different transmission distances, and the results of the mutual inductance calculated values with the simulated and experimental error values are shown in Table 2.

Analyzing the data in Table 2, it can be seen that when the transmission distance between the transmitting coil and the receiving coil is within 10–100 mm, the simulation error ε_1 of the mutual inductance value is maximal at 2.27%, and the experimental error ε_2 is maximal at 3.12%, and there is a high degree of conformity between the calculated value, the simulated value, and the experimental value.

Figure 12 shows the variation of mutual inductance values at different transmission distances plotted based on the data in Table 2. Observing Fig. 12, it can be noted that when the transmission distance between the receiving and transmitting sides is minimal, the mutual inductance reaches its maximum value. As the transmission distance increases, the mutual inductance gradually decreases. This is because as the transmission distance increases, the magnetic flux density decreases, resulting in a smaller magnetic flux in the receiving coil. Therefore, the mutual inductance is approximately inversely proportional to the transmission distance.

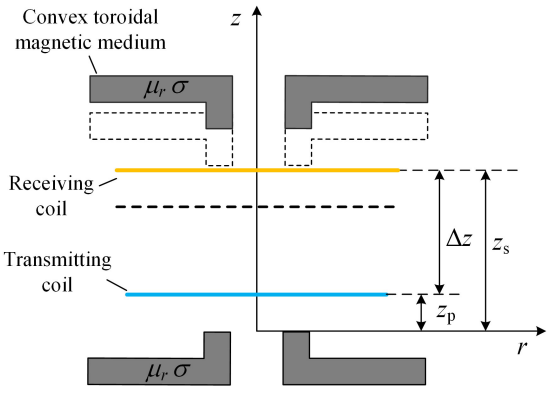

Fig. 11 Schematic of various transmission distances.

Table 2. Inductance values and errors at different transmission distances.

Δz (mm)	M_s (μH)	M_e (μH)	M_c (μH)	ε_1	ε_2
10	17.8868	17.4979	17.7292	0.89%	1.30%
20	13.1848	12.8047	13.2171	0.24%	3.12%
30	10.0934	9.9253	10.1615	0.67%	2.32%
40	7.9031	7.7624	7.9721	0.87%	2.63%
50	6.3084	6.2658	6.3461	0.59%	1.26%
60	5.0976	5.0777	5.1091	0.23%	0.61%
70	4.1553	4.1702	4.1515	0.09%	0.45%
80	3.4251	3.3106	3.4004	0.73%	2.64%
90	2.8461	2.7910	2.8050	1.47%	0.50%
100	2.3817	2.3080	2.3288	2.27%	0.89%

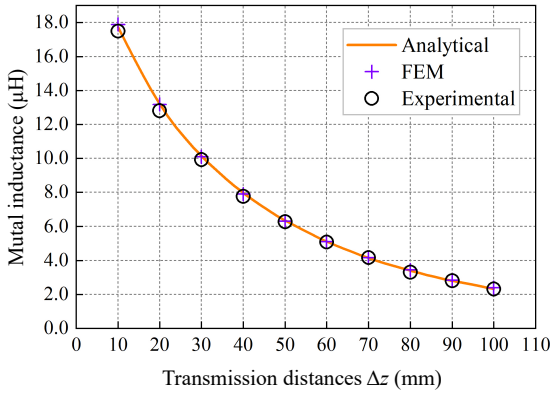

Fig. 12 Graph of inductance variation at different transmission distances.

Horizontal misalignment at different distances

In experiments conducted at different horizontal misalignment distances, it is stipulated that the receiving and transmitting sides are coaxially aligned, and the receiving coil and magnetic medium are moved along the horizontal direction with a step size of 10 mm. The initial height of the receiving coil is fixed at z_2 = 62 mm, and the mutual inductance values are recorded gradually as Δd ranges from −50 to 50 mm. Figure 13 illustrates the schematic diagram of the model at different horizontal misalignment distances, and the error results between the calculated mutual inductance values and the simulated and experimental values are shown in Table 3.

Analyzing the data in Table 3, it can be seen that when the horizontal misalignment distance of the receiver side is within −50 to 50 mm, the simulation error ε_1 of the mutual inductance value is 2.69% at maximum, and the experimental error ε_2 is 4.23% at maximum, and the mutual inductance calculated value shows good consistency with the simulation and experimental values.

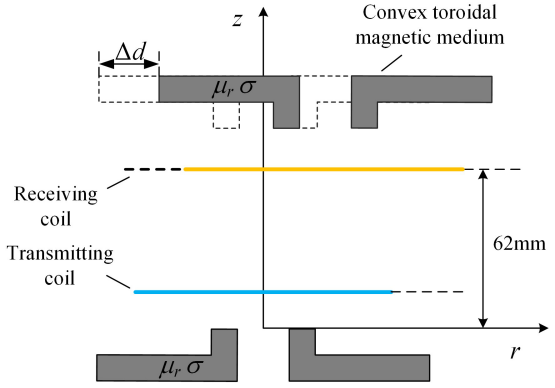

Fig. 13 Schematic diagram of horizontal misalignment.

Table 3. Inductance values and errors at horizontal misalignment.

Δd (mm)	M_s (μH)	M_e (μH)	M_c (μH)	ε_1	ε_2
−50	4.3656	4.2280	4.3171	1.12%	2.06%
−40	4.9752	4.8559	4.8450	2.69%	0.23%
−30	5.5096	5.4329	5.6536	2.55%	3.90%
−20	5.9312	5.8920	6.0063	1.25%	1.90%
−10	6.2088	6.1459	6.1930	0.26%	0.76%
0	6.3084	6.2658	6.3461	0.59%	1.26%
10	6.2060	6.1259	6.1930	0.21%	1.08%
20	5.9287	5.8404	6.0063	1.29%	2.76%
30	5.5065	5.4160	5.6536	2.60%	4.23%
40	4.9683	4.8462	4.8450	2.55%	0.03%
50	4.3630	4.2359	4.3171	1.06%	1.88%

Figure 14 is a graph of the variation of mutual inductance values at different distances of horizontal misalignment. Observing Fig. 14, it can be seen that when the height of the receiving coil is kept constant at 62 mm, the mutual inductance value is in a left-right symmetric shape about the horizontal misalignment distance of the receiving side. The mutual inductance value reaches the maximum when the misalignment distance along the horizontal of the receiving side is the smallest. With the increase of the horizontal misalignment distance, the mutual inductance value decreases gradually. This is because the magnetic field distribution makes the magnetic flux across the receiving coil is smaller when the horizontal misalignment distance is larger, resulting in the mutual inductance value showing a decreasing trend.

Variation of turns

The inner radius r_s of the receiving coil was set to 40 mm, the number of turns of the receiving-side coil was changed, and other parameters were kept consistent with Table 1. The mutual inductance value of the receiving coil is measured when the number of turns N_s is varied from six turns to 15 turns at the transmission distance Δz = 50 mm. Table 4 shows the error analysis of the calculated values of mutual inductance with respect to the simulated and experimental values when the number of turns is varied.

Analyzing the data in Table 4, it can be seen that the simulation error ε_1 of the mutual inductance value does not exceed 2.98% and the experimental error ε_2 does not exceed 3.63% when the number of turns of the coil on the receiving side is varied, and the mutual inductance calculation value shows good consistency with the simulation and experimental values. Based on the data in Table 4, the variation curves of mutual inductance values for the number of turns of the coil on the receiving side from six turns to 15 turns

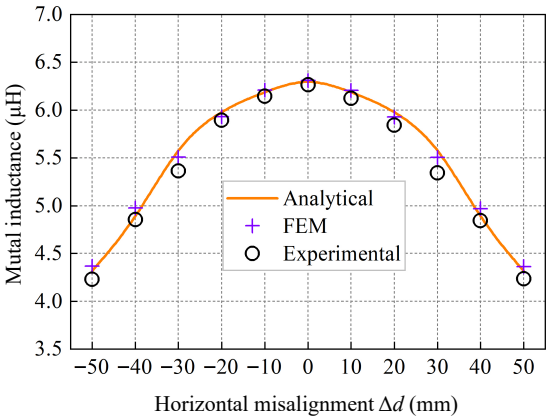

Fig. 14 Graph of inductance variation with different horizontal misalignment distances.

Table 4. Mutual inductance values and errors when changing the number of N_s.

N_s	M_s (μH)	M_e (μH)	M_c (μH)	ε_1	ε_2
6	2.3982	2.3454	2.3927	0.23%	1.98%
7	2.9411	2.9163	3.0137	2.41%	3.23%
8	3.5225	3.4263	3.5554	0.93%	3.63%
9	4.1412	4.0136	4.1311	0.24%	2.85%
10	4.7921	4.6726	4.7387	1.13%	1.39%
11	5.4730	5.3113	5.3760	1.80%	1.20%
12	6.1956	6.1184	6.0401	2.57%	1.30%
13	6.9220	6.7356	6.7283	2.88%	0.11%
14	7.6679	7.4002	7.4462	2.98%	0.62%
15	8.4281	8.3281	8.1980	2.81%	1.59%

when the transmission distance is 50 mm are plotted, as shown in Fig. 15.

Analyzing Fig. 15 shows that the slope of the mutual inductance value vs the number of turns varies with a slight upward trend. This is because, as the number of turns of the receiving coil increases, not only does the magnetic chain increase proportionally, but also the coupling area between the receiving side and the transmitting side increases due to the helical winding structure of the coil, increasing the slope.

Comparison of mutual sense when convex ring structure and disc-type structure

The magnetic media proposed in this paper adopts a convex toroidal structure, which can save nearly 15% of the magnetic media material compared with the disc-type magnetic media of the same specification. To compare the differences in the effects of the two magnetic media structures on mutual inductance with the same coil shape, experimental models of convex toroidal and disc-type magnetic media are established using the parameters in Table 1. The experimental data of the two models are measured for the horizontal misalignment distance Δd = 25 and 50 mm cases on the receiver side and Δz changes from 0 to 100 mm, respectively, and the mutual inductance scaling factor is defined:

$$\gamma = \frac{M_{e1}}{M_{e2}} \times 100\% \tag{48}$$

where, M_{e1} is the experimental mutual inductance value for the convex toroidal magnetic medium structure and M_{e2} is the experimental mutual inductance value for the disc-type magnetic medium structure. The experiments for both are conducted under the conditions depicted in Fig. 16, with the experimental setup shown in Fig. 9d.

The corresponding experimental mutual inductance values and proportion coefficients between the convex toroidal structure and the disc-type structure are listed in Table 5. The data in Table 5 show that when the horizontal misalignment distance Δd = 25 mm on the receiving side, the mutual inductance under the convex toroidal dielectric structure can reach more than 98.26% of the mutual inductance of the disc-type dielectric structure. When the horizontal misalignment distance is increased to 50 mm, the mutual inductance data of the two structures are still close to each other, and the mutual inductance of the convex toroidal dielectric structure can reach more than 97.75% of the mutual inductance of the disc-type media structure. The mutual inductance comparison data in Table 5 can be described by a scatter plot, as shown in Fig. 17.

Analyzing Table 5 & Fig. 17, it can be seen that with the convex toroidal magnetic media being able to save nearly 15% of the magnetic media material, for different transmission distances and horizontal misalignment distances, the convex toroidal structure can achieve a similar effect as the disc-type structure in terms of mutual inductance enhancement, which reflects the superiority of the convex toroidal magnetic media structure.

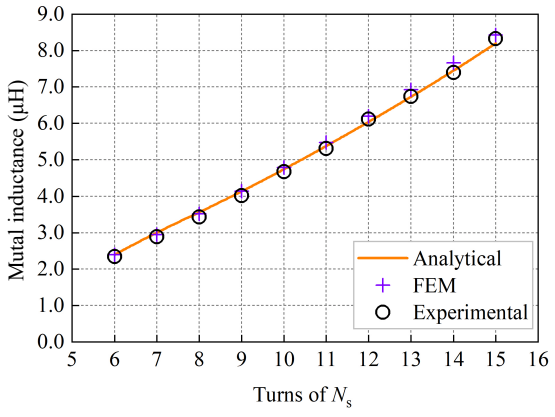

Fig. 15 Mutual inductance change with change in N_s.

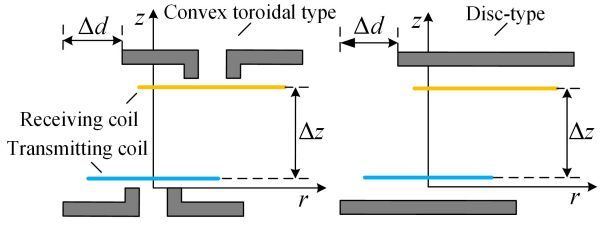

Fig. 16 Experimental conditions for two magnetic media structures.

Time comparison

With the same computer hardware configuration (CPU: i5-13600k, RAM: 16GB), the mutual inductance values of the same parameter model were obtained using the Matlab program and Maxwell simulation software for different transmission distances, different horizontal misalignment distances and coil turns variations. Table 6 records the comparative data of the time taken by both excluding the model building time.

Analyzing the data in Table 6 reveals that for different transmission distances and different horizontal misalignment tests, the average time required for simulation is 237.2 s, while the longest aver-

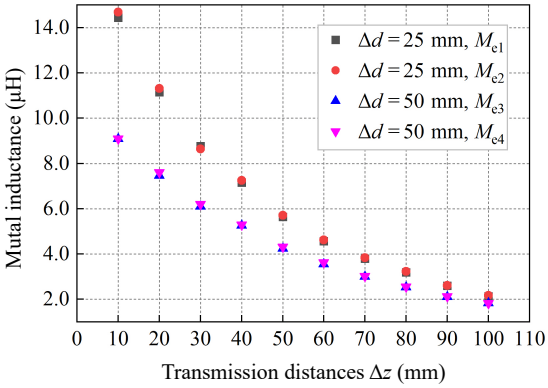

Fig. 17 Comparison of inductance between convex toroidal and disc-type magnetic media structures.

Table 5. Corresponding mutual inductance values and errors for two magnetic media structures.

Δz (mm)	Δd = 25 mm			Δd = 50 mm		
	M_{e1} (μH)	M_{e2}(μH)	γ	M_{e1}(μH)	M_{e2}(μH)	γ
10	14.4329	14.6878	98.26%	9.0775	9.0925	99.84%
20	11.1521	11.31451	98.56%	7.4525	7.6125	97.90%
30	8.7612	8.6462	98.67%	6.0875	6.1975	98.23%
40	7.1582	7.2475	98.77%	5.2530	5.2925	99.25%
50	5.6380	5.7125	98.70%	4.2377	4.3170	98.16%
60	4.5627	4.6144	98.88%	3.5525	3.6344	97.75%
70	3.7967	3.8312	99.10%	2.9925	3.0250	98.93%
80	3.1946	3.2271	98.99%	2.5226	2.5558	98.70%
90	2.5934	2.6147	99.19%	2.1061	2.1232	99.19%
100	2.1293	2.1637	98.41%	1.8254	1.8325	99.61%

Table 6. Calculating the average time required for mutual inductance.

Experiment type	Algorithm time (s)	Simulation time (s)
Transmission distances	3.102	237.2
Horizontal misalignment	3.375	245.4
Adding one more coil	0.047	13.35

Table 7. Comparison of mutual inductance calculation methods with other literature.

Method	DTD	DHMD	MM	FMS	DS	MS	ERR	Ref.
Elliptic integral	√	√	×	×	×	×	/	[12]
Bessel integral	√	√	×	×	×	×	/	[13]
Euler angles	√	√	×	×	×	×	/	[15]
Fourier-Bessel transform	√	√	√	×	√	×	/	[17]
Coordinate transformation method	√	√	√	√	×	×	4.78%	[18]
Truncation domain division	√	√	√	√	×	×	4.76%	[20]
Magnetic circuit magnetic resistance theory	√	×	√	√	√	×	8.13%	[21]
Magnetic vector potential position equivalence method	√	√	√	√	√	√	4.23%	This study

DTD: different transmission distances; DHMD: different horizontal misalignment distances; MM: magnetic medium; FMS: finite magnetic medium; DS: double side; MS: Material Saving; ERR: Error. DS means the magnetic medium is bilateral case, MS means saving the magnetic medium material, ERR means the maximum calculation error.

age time required using the provided algorithm is 3.375 s. This indicates that the calculation speed using the algorithm is approximately 70 times faster than the simulation. In the test with varying numbers of turns, adding one turn to the coil increases simulation time by 13.35 s, while the algorithm time only increases by 0.047 s. Therefore, the method proposed in this paper demonstrates a significant advantage in mutual inductance calculation speed.

Comparison of mutual sense calculation methods in the national and international research literature

The model calculation method proposed in this paper is compared with other domestic and international literature, and the comparison results are shown in Table 7.

Table 7 shows that the proposed magnetic vector position equivalence method in this paper can effectively calculate the mutual inductance in wireless power transfer systems containing bounded magnetic media, relative to studies by Babic et al.[12], Conway[13], Liu et al.[15], and Liu et al.[17]. Additionally, compared to studies by Zhang et al.[18] and Chen et al.[20], it can calculate mutual inductance in systems containing bilateral bounded magnetic media. Furthermore, compared to reference[21], it can calculate the mutual inductance on the receiving side with a horizontal misalignment of bilateral bounded magnetic media. Moreover, only the method proposed in this paper can effectively calculate mutual inductance while saving bilateral magnetic media materials, and the maximum error is 4.23%, which is within the acceptable range.

Conclusions

This paper proposes a method of magnetic vector potential position equivalence and derives analytical solutions for mutual inductance of circular coils with bilateral bounded convex magnetic material rings. This method is based on Maxwell's equations and boundary conditions, utilizing the magnetic vector potential to derive the mutual inductance calculation formula for the coaxial case. Building upon this, the method employs the position equivalence approach to derive the mutual inductance calculation formula for horizontal misalignment.

Through verification on both finite element simulation and experimental platforms, it is demonstrated that the mutual inductance calculation errors for different transmission distances, various horizontal misalignments and changes in the number of turns do not exceed 4.23%. Additionally, the computational speed is 70 times faster than simulation, affirming the effectiveness and efficiency of the proposed method. Under equivalent specifications, the proposed model structure can save 15% of material compared to using a disc-type magnetic material structure.

The proposed mutual inductance calculation method can be used for the design and optimization of coil parameters in wireless power transfer systems, and the proposed convex annular magnetic dielectric structure can be used in penetrating wireless power transmission scenarios such as pipelines.

Author contributions

The authors confirm contribution to the paper as follows: study conception and design: Hu C, Li Z; data collection: Hu C, Kong L; analysis and interpretation of results: Hu C, Wang J; draft manuscript preparation: Hu C, Zhang C. All authors reviewed the results and approved the final version of the manuscript.

Data availability

The datasets generated during the current study are available from the corresponding author on reasonable request.

Acknowledgments

This research is partially funded by National Key R&D Program of China (2022YFB3403200), Hunan Provincial Department of Education Key Project (23A0432), Hunan Provincial Natural Science Foundation (2022JJ30226), Outstanding Youth Project of Scientific Research Program of Hunan Provincial Department of Education (22B0577) and National Natural Science Foundation of China Youth Science Fund Project (62303178).

Conflict of interest

The authors declare that they have no conflict of interest.

Dates

Received 5 May 2024; Revised 15 July 2024; Accepted 2 August 2024; Published online 3 September 2024

References

1. Cai C, Wang J, Liu R, Fang Z, Zhang P, et al. 2019. Resonant wireless charging system design for 110-kV high-voltage transmission line monitoring equipment. *IEEE Transactions on Industrial Electronics* 66:4118–29
2. Nguyen VT, Pawaskar VU, Gohil G. 2021. Isolated gate driver for medium-voltage sic power devices using high-frequency wireless power transfer for a small coupling capacitance. *IEEE Transactions on Industrial Electronics* 68:10992–1001
3. Barmada S, Musolino A, Zhu J, Yang S. 2023. A novel coil architecture for interoperability and tolerance to misalignment in electric vehicle WPT. *IEEE Transactions on Magnetics* 59:8600205
4. Liu X, Gao F, Niu H, Sun G, Wang T, et al. 2024. A series–parallel transformer-based WPT system for 400-V and 800-V electric vehicles with Z1 or Z2 class. *IEEE Transactions on Power Electronics* 39:1749–61

5. Park C, Park J, Shin Y, Kim J, Huh S, et al. 2020. Separated circular capacitive coupler for reducing cross-coupling capacitance in drone wireless power transfer system. *IEEE Transactions on Microwave Theory and Techniques* 68:3978–85
6. Wu S, Cai C, Liu X, Chai W, Yang S. 2022. Compact and free-positioning omnidirectional wireless power transfer system for unmanned aerial vehicle charging applications. *IEEE Transactions on Power Electronics* 37:8790–94
7. Cheng Z, Lei Y, Song K, Zhu C. 2015. Design and loss analysis of loosely coupled transformer for an underwater high-power inductive power transfer system. *IEEE Transactions on Magnetics* 51:8401110
8. Sasatani T, Sample AP, Kawahara Y. 2021. Room-scale magnetoquasistatic wireless power transfer using a cavity-based multimode resonator. *Nature Electronics* 4:689–97
9. Narayanamoorthi R. 2019. Modeling of capacitive resonant wireless power and data transfer to deep biomedical implants. *IEEE Transactions on Components, Packaging and Manufacturing Technology* 9:1253–63
10. Yi X, Zheng W, Cao H, Wang S, Feng X, et al. 2021. Wireless power transmission for implantable medical devices using focused ultrasound and a miniaturized 1-3 piezoelectric composite receiving transducer. *IEEE Transactions on Ultrasonics, Ferroelectrics, and Frequency Control* 68:3592–98
11. Compter J. 2019. Mutual inductance and forces between two non-coaxial co-planar circular thin-wall air coils. *COMPEL - The international journal for computation and mathematics in electrical and electronic engineering* 38:216–31
12. Babic S, Sirois F, Akyel C, Lemarquand G, Lemarquand V, et al. 2011. New formulas for mutual inductance and axial magnetic force between a thin wall solenoid and a thick circular coil of rectangular cross-section. *IEEE Transactions on Magnetics* 47:2034–44
13. Conway JT. 2007. Inductance calculations for noncoaxial coils using Bessel functions. *IEEE Transactions on Magnetics* 43:1023–34
14. Hurley WG, Duffy MC, Zhang J, Lope I, Kunz B, et al. 2015. A unified approach to the calculation of self- and mutual-inductance for coaxial coils in air. *IEEE Transactions on Power Electronics* 30:6155–62
15. Liu S, Su J, Lai J, Zhang J, Xu H. 2021. Precise modeling of mutual inductance for planar spiral coils in wireless power transfer and its application. *IEEE Transactions on Power Electronics* 36:9876–85
16. Hurley WG, Duffy MC. 1997. Calculation of self- and mutual impedances in planar sandwich inductors. *IEEE Transactions on Magnetics* 33:2282–90
17. Luo Z, Wei X. 2018. Analysis of square and circular planar spiral coils in wireless power transfer system for electric vehicles. *IEEE Transactions on Industrial Electronics* 65:331–41
18. Zhang X, Quan C, Li Z. 2021. Mutual inductance calculation of circular coils for an arbitrary position with electromagnetic shielding in wireless power transfer systems. *IEEE Transactions on Transportation Electrification* 7:1196–204
19. Yi J, Yang P, Li Z, Kong P, Li J. 2023. Mutual inductance calculation of circular coils for an arbitrary position with a finite magnetic core in wireless power transfer systems. *IEEE Transactions on Transportation Electrification* 9:1950–59
20. Dong Z, Li X, Liu S, Xu Z, Yang L. 2021. A novel all-direction antimisalignment wireless power transfer system designed by truncated region eigenfunction expansion method. *IEEE Transactions on Power Electronics* 36:12456–67
21. Chen Y, Chen K, Zheng S, Jiang Y, Yuan L, et al. 2023. Analytical modeling method for inductance of planar magnetic coupler in wireless power transfer. *Proceedings of the CSEE* 43(4):1504–16
22. Rituraj G, Kumar P. 2021. A new magnetic structure of unipolar rectangular coils in WPT systems to minimize the ferrite volume while maintaining maximum coupling. *IEEE Transactions on Circuits and Systems II: Express Briefs* 68:2072–76
23. Li H, Wang C, Wei Z, Li D. 2019. Research of shield structure for wireless power transfer system. *Advanced Technology of Electrical Engineering and Energy* 38(5):74–83